Deuterium Exchange Mass Spectrometry as a Probe of Protein Kinase Activation. Analysis of Wild-Type and Constitutively Active Mutants of MAP Kinase Kinase-1†

Katheryn A. Resing* and Natalie G. Ahn‡

Department of Chemistry and Biochemistry, and Howard Hughes Medical Institute, University of Colorado, Boulder, Colorado 80309

Received July 18, 1997; Revised Manuscript Received September 5, 1997⊗

ABSTRACT: Wild-type and constitutively active mutants of human MAP kinase kinase-1 (MKK1) were analyzed by deuterium exchange mass spectrometry using a protocol that minimized loss of deuterium during analysis due to back exchange. The observed peptides accounted for 335 out of 393 residues. Not counting overlap peptides, three peptides showed decreased exchange in constitutively active compared to wild-type MKK1 and nine showed increased exchange. Backbone amides in which exchange rates decreased upon kinase activation were observed near the regulatory phosphorylation sites Ser218 and Ser222 and the adjacent β9 strand. These decreases are consistent with electrostriction or reduced solvent access due to domain closure or formation of new hydrogen or salt bonds around the catalytic cleft and within the activation lip. Increased exchange upon activation was observed within six peptides derived from helix C and the five-stranded β sheet from the N-proximal lobe of the conserved kinase domain and in one peptide located at the interface between the N- and C-proximal lobes. Two amides that underwent increased exchange were specifically localized between residues 68 and 69 in β1 and 140 and 142 in β5. These residues probably form contacts with each other on opposite sites of the β sheet as well as with helix C. These increases appeared to represent localized fluctuations, rather than rigid body rearrangements, suggesting that MKK1 activation requires enhanced flexibility within the N-proximal lobe, perhaps to accommodate ATP binding, phosphotransfer, or ADP release.

MAP kinase kinase-1 (MKK1)[1] phosphorylates and activates the MAP kinases, ERK1 and ERK2, in the MAP kinase cascade, a signaling pathway that regulates mammalian cell growth and differentiation (*1*, *2*). Defining the molecular basis of conversion of this kinase from its inactive to active state is important in understanding the regulation of MKK1. MKK1 can be activated in vitro by upstream kinases, Raf-1, c-Mos, or MEK kinase (MEKK); these directly phosphorylate MKK1 at residues Ser_{218} and Ser_{222}, which are located near the active site within a loop between subdomains 7 and 8 of the conserved kinase core (*3*−*5*). This loop is often referred to as the activation lip because phosphorylation in this region is involved in the activation of many kinases.

Activation of MKK1 can be accomplished by two types of mutations. Substitution of the phosphorylated residues to Ser_{218}Glu and Ser_{222}Asp yields a mutant with 80-fold greater basal activity than wild-type, most likely due to enhanced negative charge within the activation loop (*6*, *7*). Deleting residues 44−51 in MKK1 (ΔN4) results in 100-fold enhanced activity due to perturbations in secondary structure at the N-terminus (*7*). Together, these two mutations synergistically elevate V_{max}/K_m with respect to both ATP and ERK2 substrates, mimicking the effect of phosphorylation on wild-type MKK1.

X-ray structural analyses of several protein kinases predict two types of conformational changes following activation by phosphorylation within the activation lip (*4*, *5*, *8*). First, reconfiguration of the lip upon phosphorylation may lead to stabilizing interactions between the lip and active site residues, optimizing the orientation of residues involved in substrate binding and catalysis. Second, rotation of the two major lobes with respect to each other may lead to closure of the catalytic cleft. Dynamic motion is also an important aspect of catalysis (*9*, *10*); however, because crystallographic data provide averaged minimum energy structures, dynamic motions cannot be observed.

Hydrogen exchange rates between peptide backbone amide nitrogen atoms and solvent are often used to probe solution dynamic motions of proteins (*11*, *12*). Accurate measurements of exchange rates of individual amides with deuterated

† Supported by NIH Grants AR39730 (K.A.R.) and GM48521 (N.G.A.) and the Searle Scholar's Foundation (N.G.A.).

* Corresponding author; Department of Chemistry and Biochemistry.

‡ Howard Hughes Medical Institute. Address reprint requests to N.G.A. at Department of Chemistry and Biochemistry, Campus Box 215, University of Colorado, Boulder, CO 80309.

⊗ Abstract published in *Advance ACS Abstracts,* December 15, 1997.

[1] Abbreviations: cAPK, cyclic AMP dependent kinase; CID, collision-induced dissociation; ERK, extracellular signal regulated kinase; ESI-MS, electrospray ionization mass spectrometry; HPLC, high performance liquid chromatography; LC/MS, reversed phase HPLC coupled to mass spectrometry; MKK, MAP kinase kinase (WT, wild-type; S218E/S222D, replacement of phosphorylation sites with acidic residues; ΔN4, deletion of residues 44−51; G1C, ΔN4/S218E/S222D); MS/MS, tandem mass spectrometry; NMR, nuclear magnetic resonance; TFA, trifluoroacetic acid.

S0006-2960(97)01750-9 CCC: $15.00
Published on Web 01/13/1998

water can be obtained by NMR (*13*). However, because NMR is limited to small, highly purified proteins that are soluble at high concentrations, this technique is most often applied to protein folding dynamics, and few studies exist that probe dynamic changes that occur with large (>20 kDa) regulatable enzymes upon activation.

Recent use of mass spectrometry to carry out deuterium exchange experiments has enabled measurement of rates within larger proteins. Backbone amide exchange rate information is obtained by examining mass increases within local regions of the protein, acquired by proteolysis after exposure to D_2O (*14*−*16*). In this study, constitutively active mutants of MKK1 are compared with WT-MKK1 by deuterium exchange electrospray mass spectrometry. The results provide evidence for localized changes in solvent accessibility in MKK1, reflecting increased flexibility or dynamic motions accompanying enhanced catalytic activity, as well as expected decreases in solvent accessibility near the activation lip.

MATERIALS AND METHODS

Protein Preparation. Histidine-tagged wild-type and mutant human MKK1 were expressed in *Escherichia coli* and purified by Ni^{2+}-nitrilotetraacetic acid and DEAE-Sephacel chromatography as previously described (*17*). The N-terminal histidine tag was removed by proteolysis with enterokinase resulting in an N-terminus with the sequence $DRWGSGGVGSALPGSKM_1$. The protein was desalted and further purified by gel filtration (Superose 12 10/30HR, Pharmacia) in 10 mM potassium phosphate, pH 8, 50 mM KCl, and 1 mM dithiothreitol. Eluted protein was concentrated 4.3-fold by speed-vac centrifugation, and frozen at −80 °C in 50 μL aliquots. Each aliquot was sufficient for five deuterium exchange mass spectrometric analyses and was used within 3 h of thawing. To eliminate systematic day-to-day bias, aliquots of mutant and wild-type enzymes were analyzed randomly. Comparison of proteolyzed and unproteolyzed MKK1 showed no major differences in deuterium exchange results (data not shown).

Deuterium Exchange. MKK1 activity is unstable upon lyophilization; therefore, in-exchange was initiated by pipetting 10 μL of MKK1 at 0 °C into 90 μL of D_2O (Sigma) at 10 °C in polyethylene Titertubes (Bio-Rad) using a pipetter (P20, Gilson) to minimize shear forces on the protein. At various times, tubes were transferred to a −15 °C salt water bath, and 5 s later, 90 μL of quench buffer (25 mM citrate and 25 mM succinate, pH 2.4, at 0 °C) was added. After 20 s, the tube was transferred to ice, and 10 μL of 0.4 mg/mL pepsin (Sigma, dissolved in water and stored in aliquots at −80 °C) was added to each sample using an ice-cold HPLC injection syringe wrapped with insulating material and fitted with a wide bore needle. The sample was then drawn into the same syringe and loaded into a 1 mL polyether ether ketone (PEEK) injection loop (Rheodyne) that was rinsed with 0 °C H_2O before loading. The HPLC injection loop, a solvent precooling coil, and the column (directly attached to the injection loop) were completely submerged in an ice/water slurry, tightly packed to minimize small variations in temperature.

One minute after protease addition, the injector loop was turned to the inject position, loading the digest at 40 μL/min onto a self-packed 500 μm capillary HPLC column (11−16 cm, POROS R120, PerSeptive) equilibrated in 0.05% trifluoroacetic acid (TFA). Sample loading required 5 min; the injection loop was then returned to the load position, washed with water at 0 °C, and loaded with a step gradient (18 μL each of 5, 7.5, 10, 12.5, 15, 20, 30, 40, and 50% acetonitrile, 0.05% TFA). After a 6 min column wash, the injection valve was switched to allow the gradient to flow through the column at 20 μL/min and the column was connected to the mass spectrometer for data collection. Peptide elution was complete after 10 min; thus, 23 min elapsed between initiation of digestion and complete data collection. Preferential loss of deuterated forms resulted in artefactually lower mass and low peptide recovery at longer incubation times. This was more pronounced with wild-type than constitutively activated MKK1 mutants and was minimized by carrying out the incubations at 10 °C for no more than 4 h.

Mass Analysis and Peptide Sequencing. Mass determinations were performed on an API-III^+ triple quadrupole mass spectrometer (Perkin Elmer Sciex), with the plenum chamber at 21 °C. The detector was calibrated to unit resolution with polypropylene glycol; this results in a mass accuracy of at least 0.15 Da for a 1200 Da peptide (the average size of peptides in this study). Data were collected at an orifice voltage of 75 V, scanning a 0.1 Da/e window from 325 to 1400 Da/e with 0.5 ms dwell time (5.9 s/scan). Peptides were identified by MS/MS sequencing conducted "on-the-fly" as peptides eluted from the capillary column (LC/MS/MS) as previously described (*18*), following pepsin proteolysis under conditions identical to those used for the deuterium exchange experiments, except that D_2O was omitted. Analysis of MS and MS/MS spectra utilized Sciex software; data were plotted for publication using Cricket Graph or Sigmaplot programs.

In-Exchange Controls. The extent of in-exchange that occurred after acidification (IE control) was measured by adding D_2O to protein after addition of quench buffer. A total of 10 μL of protein was added to 90 μL of quench buffer at 0 °C. Then, 90 μL of D_2O at 10 °C was transferred to the −15 °C bath, followed by immediate addition of the acidified 0 °C protein sample, and the analysis was carried out as described above. Artefactual deuterium incorporation was less than the error in total in-exchange (4−5%) and was therefore ignored during data analysis.

Back-Exchange Controls. Back-exchange to hydrogen is usually measured by heating the protein to achieve 100% in-exchange and then measuring the subsequent loss of deuterium during analysis. However, heating these low concentrations of MKK1 in D_2O led to almost complete loss of protein. Therefore, back-exchange was measured by incubating a peptide digest of MKK1 in D_2O to achieve 100% in-exchange, then analyzing this digest as for deuterated MKK1, except without adding pepsin. Undeuterated peptides were generated by diluting 50 μL of protein with 50 μL of H_2O and digestion with 10 μL of 0.4 mg/mL pepsin as described for the experimental samples. Peptides were loaded onto the HPLC column and batch eluted at 40% acetonitrile and 0.05% TFA. Following lyophilization, peptides were dissolved in 30 μL of 45 mM potassium phosphate, 150 mM KCl, and 4 mM dithiothreitol, pH 8.0, in water and 270 μL of D_2O and heated at 90 °C for 90

min. Deuterated peptides were reloaded onto the HPLC column and analyzed for mass incorporation by LC/MS protocol used for deuterated time points. Back-exchange was estimated by peptide mass, after normalizing to 100% deuterium. The back-exchange could only be measured for a subset of the 41 peptides used in the deuterium exchange experiments. For the other peptides, back-exchange was taken as the average of those observed (12%).

Data Analysis. Peptide ions were located by scanning for the predicted masses (extract ion scan); intensities of all scans containing the peptide were summed to produce a spectrum for each ion. In some cases, only the front or the back half of an eluting peptide peak was analyzed in order to avoid nearby contaminants. Resulting ion spectra were smoothed 3−10 times, using PE Sciex software. The mass of the MH^+ ions were determined as the weighted average mass of the isotope peaks, assuming the sequence-predicted masses for each isotope peak. Masses of MH_2^{2+} and MH_3^{3+} (where isotope peaks were not resolved) were measured by centroiding at half-height of the observed peak. When more than one charged form of a peptide was present, the masses measured for each ion were averaged.

Data sets were discarded when the singly charged ions showed isotope peaks that fit poorly to a binomial distribution or when masses of all peptides within the set systematically deviated from fitted time courses for each peptide. In most cases, these deviations could be explained by variations in sample handling. In 15% of data sets, a small drift in calibration was detected as slightly incorrect masses for the isotope peaks of MH^+ ions (<0.15 Da/e); the true masses of these ions were used to formulate a correction curve for those data sets.

Progress curves for individual peptides were fit using Sigmaplot to the sum of two exponentials from the following expression:

$$y = N - Ae^{-k_1 t} - Be^{-k_2 t}$$

where y = observed peptide mass at time t; N = peptide mass at maximal in-exchange of deuterium (90%); A = the number of amides undergoing exchange with fast rate constant k_1 (>1.0 min^{-1}); B = the number of amides undergoing exchange with intermediate rate constant k_2 (0.001−1.0 min^{-1}). The number of amides (C) undergoing exchange at slower rate constants (k_3 < 0.001 min^{-1}) was calculated by subtracting the peptide mass at maximal in-exchange ($A + B$) from the theoretical mass at infinite in-exchange (Y_∞). Y_∞ is equal to the total number of backbone amides in a peptide, excluding proline residues. Most data sets fit within 10 iterations, with standard errors generally less than 15% for the A and B parameters and less than 35% for the k_1 and k_2 parameters. Peptides of low intensity yielded parameters with greater errors and were often sensitive to back-exchange and in-exchange. In some cases with large and/or weakly ionizing peptides, where the errors in individual data points were large, there were significant differences between WT vs mutant MKK1 fitted parameters, although the fitted curves looked identical. In these cases, each set of parameters fit either data set equally well; therefore, in the analysis of the WT-MKK1 data sets, values of N and/or k_1 were fixed to those in the corresponding G1C data sets, resulting in nearly identical fits for the other parameters (indicated as footnotes to Table 1).

Homology Modeling of MKK1. The Biopolymer and Builder modules of the Insight II 95.0 program were used to model the peptide backbone of human MKK1 (Leu_{42} to Thr_{386}) from the X-ray coordinates of mouse cAMP-dependent protein kinase (Val_{15} to Lys_{319}) in the closed ternary conformation (2CPK, *19*) with the following insertions or deletions: (1) Ala_{38} and Asp_{41} in cAPK were replaced with Asp_{65} and Asp_{66} from MKK1, deleting cAPK residues Gln_{39} and Leu_{40}; (2) Lys_{78} and Lys_{81} in cAPK were replaced with Ile_{103} and Lys_{104} in MKK1, deleting Val_{79} and Val_{80}; (3) Leu_{160} and Asp_{161} of cAPK were replaced with Lys_{183} and Lys_{185} of MKK1, inserting His_{184} in MKK1; (4) Thr_{195} and Trp_{196} of cAPK were replaced with Met_{219} and Asn_{221} of MKK1, inserting Ala_{220} in MKK1; (5) residues Pro_{265} to Pro_{306} of MKK1 were deleted, replacing residues Phe_{239} and Ala_{240} of cAPK with Pro_{264} and Pro_{307} of MKK1; (6) Val_{255} and Arg_{256} of cAPK were replaced with Pro_{322} and Lys_{324} of MKK1, inserting Pro_{323} in MKK1; (8) His_{260} and Phe_{261} of cAPK were replaced with Gly_{328} and Phe_{330} of MKK1, inserting Val_{329} in MKK1. The model was then optimized using the Discover 3.0 program for energy minimization, with temperature 1000 K, time step 1.0, and 1900 iterations. Ribbon diagrams corresponding to the peptide backbone of cAPK and the MKK1 model were drawn by Insight II.

RESULTS

In-Exchange of Deuterium and Correction for Back-Exchange during Analysis. Deuterium exchange in MKK1 was most conveniently studied by dilution into D_2O (90% v/v). In-exchange reactions were quenched by rapid cooling and acidification followed by rapid protein digestion using pepsin, which is active at low pH. During the HPLC elution, deuterium incorporated into hydroxyl, amine, or carboxylate groups rapidly exchanges back to hydrogen. Thus, the increased peptide masses reflect deuterium exchange primarily at backbone amides where back-exchange is slow compared to the time scale of the experiment. Spatial resolution for deuterium exchange by mass spectrometry requires digestion of protein into small peptides that adequately represent the sequence and that can be resolved by reverse phase HPLC. Forty-one peptides covering 85% of the full length sequence of MKK1 were identified by LC/MS/MS sequencing (Figure 1). These ranged in length from 3 to 28 residues, averaging 11 amino acids.

Initial experiments compared deuterium exchange into wild-type MKK1 (WT) vs constitutively active ΔN4/S218E/S222D (G1C), a mutant 530-fold more active than wild-type. All peptides showed increased mass vs time in D_2O. For example, in-exchange of the MH^+ ion for peptide 13/14 is shown in Figure 2. In absence of D_2O, this ion shows a series of peaks differing by 1 Da/e, primarily due to the natural isotope distribution of $^{13}C/^{12}C$, $^{14}N/^{13}N$, or $^{34}S/^{32}S$. As the protein is incubated in D_2O, the distribution shifts to higher mass as deuterium replaces hydrogen.

Back-exchange of deuterium during analysis is a major problem in mass spectrometric exchange studies, reported from 33−50% (*15*, *20*). Our initial experiments, performed using published protocols, yielded 40−50% back-exchange; therefore, various improvements were developed as described in Materials and Methods. The most significant decrease

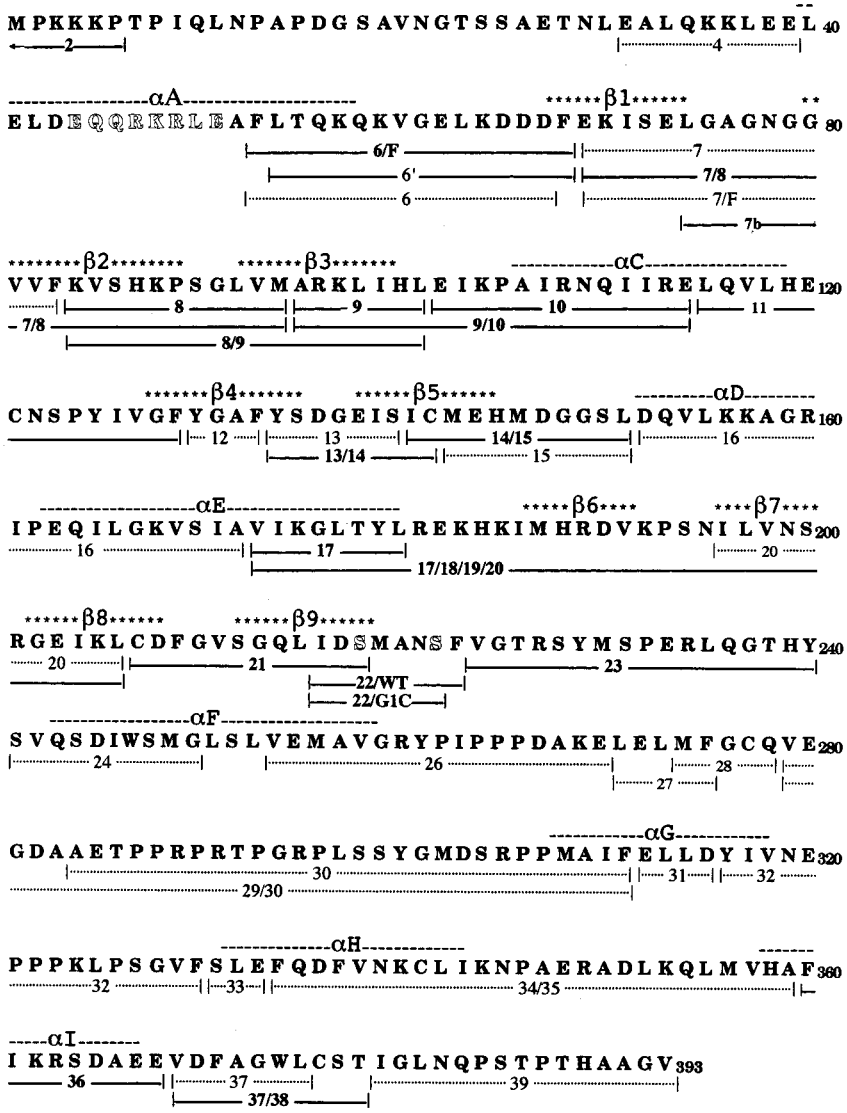

FIGURE 1: Sequence of human MKK1: Bars delineate peptides observed in this study, where solid and dotted lines represent peptides that undergo changes or no changes, respectively, in exchange rates between WT and G1C. Residues corresponding to the ΔN4 deletion and phosphorylatable residues Ser_{218} and Ser_{222} are shown in outline. Approximate locations of α helices C−I and β strands $\beta1-\beta9$ predicted from homology modeling are indicated above the sequence. Also noted is the alignment of residues 40−57 of MKK1 with helix A of cAMP-dependent kinase.

in back-exchange was achieved by digesting with pepsin in the HPLC injection loop, eliminating excessive handling. The new procedure resulted in back-exchange values averaging 12% (Table 1), and reduced artefactual in-exchange that occurred during acidification and proteolysis to 5−10% (for example, compare first two panels in Figure 2). Low back-exchange was validated by detection of high levels of deuteration in several peptides. For example, peptide 16 showed nearly complete in-exchange, and peptides 7 and 10 showed 94% and 96% deuterium incorporation, respectively, after correcting for measured back-exchange values of 15 and 12% (Table 1). It is unlikely that this high recovery can be explained by incomplete back-exchange from His or Arg side chains (*21*), because peptide 7 has neither of these residues. The back-exchange of 12 peptides lacking His or Arg averaged 14% (Table 1, Figure 1).

Hydrogen Exchange Rates. Previous measurements of deuterium incorporation by NMR, mass spectrometry, or infrared spectroscopy showed that progress curves for deuterium exchange can be fit to three-compartment models (*12*, *20*, *22*). The instability of MKK1 after several hours in D_2O precluded measurement of slow exchanging amides. For this reason, data were fit to a two-compartment model where N is the equilibrium mass and A and B are the number of amides in fast and intermediate exchanging classes, which exchange with rate constants k_1 and k_2, respectively. Least-squares fitted parameter values for each peptide observed in the digests of WT or G1C are shown in Table 1 with A and B parameters normalized to 100% D_2O and corrected for measured or estimated back-exchange rates. The number of amides in the slow class of exchanging amides (C) were calculated as the total number of exchangeable amides minus $A + B$.

Estimates of deuterium incorporation into surveyed peptides showed 68% of surveyed amide hydrogens (209/304) exchanged by the end of the 4 h incubation. Of these, 148/304 = 48% and 61/304 = 20% belonged to the fast and intermediate exchanging groups, respectively, with 32% in the slow group. These values are comparable to those reported for other proteins; for example, a recent study of

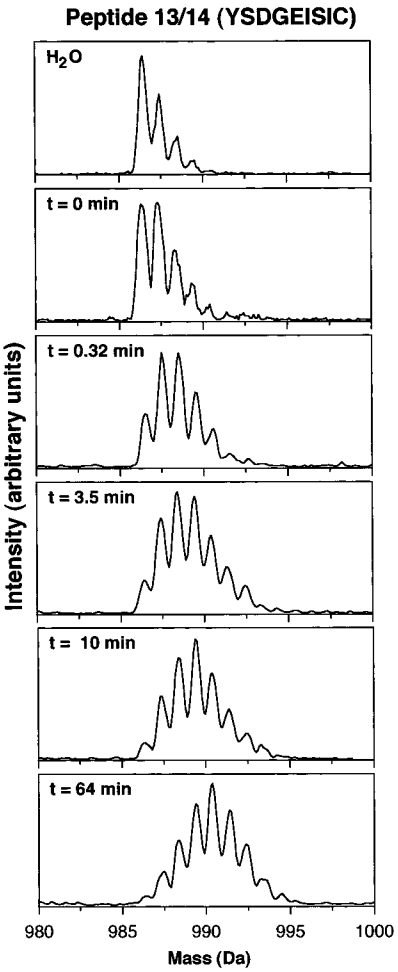

FIGURE 2: Isotope peaks from the MH^+ ion (986.1 Da/e, undeuterated mass) of peptide 13/14: Data for this peptide derived from WT show changes in mass due to increasing deuterium incorporation vs time. The first panel shows the ion derived from protein incubated in H_2O. The second panel shows the results for the in-exchange control (as described in Materials and Methods). The third panel shows the ion derived from protein incubated in D_2O for 64 min. As deuterium exchanges with hydrogen, isotope peaks approximate a binomial distribution (the smoothing program slightly "flattens" the distribution).

deuterium exchange into apolipoprotein-III (166 amino acids) by fourier transform infrared spectroscopy showed 52% fast, 12% intermediate, and 36% slow exchanging amide populations (*22*). The magnitudes of fitted rate constants were found within relatively narrow ranges around $k_1 = 2-10$ min^{-1} and $k_2 = 0.03-0.3$ min^{-1}, similar to the ranges reported by others (*12*).

For most peptides, no differences were detected between WT and G1C. However, a total of nine peptides (not counting overlapping peptides) showed increased deuterium in-exchange and three showed decreased in-exchange upon conversion from the inactive to active form of MKK1 (Figure 1, Table 1). For smaller peptides, near-integral differences were observed between WT and G1C. For example, parameter values for peptide 13/14 (Figure 3A), normalized to 100% D_2O and corrected for 21% back-exchange, were $A = 2.0$, $B = 1.8$, and $C = 4.2$ for WT and $A = 2.0$, $B = 3.0$, and $C = 3.0$ for G1C (Table 1). In this case, the rate constants remained unchanged (WT vs G1C, $k_1 = 8.5$ vs 7.4 min^{-1} and $k_2 = 0.034$ vs 0.034 min^{-1}). Thus, the data are best fit to a model where a slow exchanging amide in

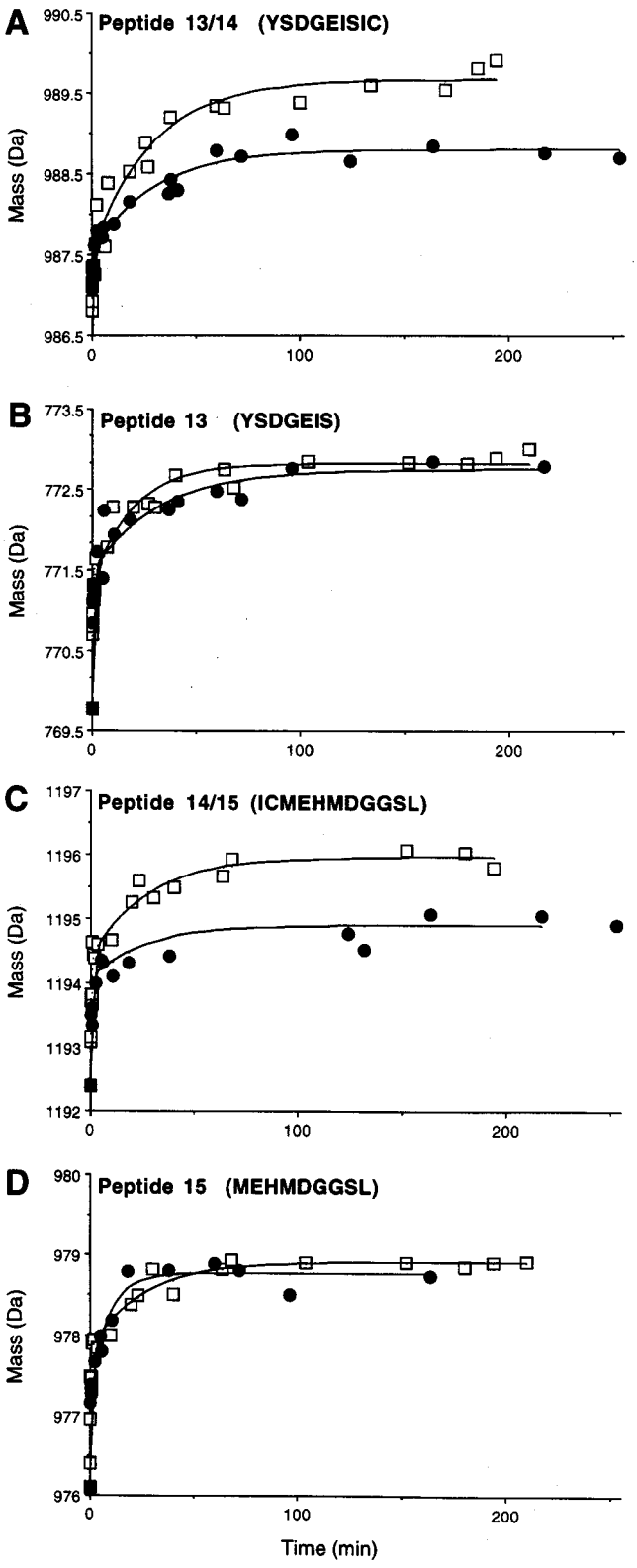

FIGURE 3: Deuterium incorporation into alternatively proteolyzed forms demonstrate that enhanced deuteration in G1C can be localized to Ile_{141}-Cys. Data are shown for (A) peptide 13/14, (B) peptide 13, (C) peptide 14/15, and (D) peptide 15 derived from WT (●) or G1C (□). Lines indicate predicted time courses derived from least squares fitted parameters (Table 1). Data points at time = 0 represent peptide average masses in H_2O. Data shown are obtained from MH^+ ions and are not normalized to 100% D_2O or corrected for back-exchange. Note that most peptides appear to be at equilibrium after 100 min.

Table 1: Least-Squares Fitted Exchange Parameters for Peptides from MKK1-WT and MKK1-G1C[a]

peptide	MKK	mass (Da)	equilibrium mass (N)	BE[b]	k_1 (min^{-1})	k_2 (min^{-1})	A[c]	B[c]	C[d]	total (Y_∞)
6/F	G1C	1911.16	1919.49 (0.20)	15%	5.94 (0.80)	0.077 (0.452)	10.4 (0.8)	0.5 (0.5)	4.1	15
	WT		1919.49[e]		5.90[e]	0.103 (0.139)	8.0 (0.8)	2.9 (0.6)	4.1	
6	G1C	1763.98	1772.64 (0.21)	9%	8.92 (1.38)	0.031 (0.014)	8.7 (0.5)	1.9 (0.3)	3.4	14
	WT		1772.42 (0.11)		9.08 (0.69)	0.032 (0.011)	8.8 (0.3)	1.5 (0.2)	3.7	
7	G1C	1623.84	1633.35 (0.21)	15%	5.23 (0.61)	0.034 (0.031)	11.1 (0.7)	1.3 (0.4)	1.6	14
	WT		1633.08 (0.12)		8.01 (1.30)	0.169 (0.134)	10.6 (0.6)	1.5 (0.4)	1.9	
7b	G1C	890.02	895.46 (0.32)[k]	12%	4.65 (1.23)	0.028 (0.060)	6.2 (0.8)	0.7 (0.5)	1.1	8
	WT		895.43 (0.04)		12.5 (1.60)	0.442 (0.115)	5.1 (0.3)	1.8 (0.2)	1.1	
8	G1C	1181.67	1187.01 (0.11)	13%	3.22 (0.35)	0.028 (0.019)	5.2 (0.3)	0.8 (0.2)	3.0	9
	WT		1186.98 (0.11)		1.45 (0.69)	0.089 (0.033)	2.8 (0.6)	3.0 (0.6)	3.2	
9	G1C	850.09	853.55 (0.06)	6%	5.86 (1.58)	0.176 (0.055)	2.1 (0.3)	2.0 (0.2)	1.9	6
	WT		853.39 (0.04)		10.4 (1.26)	0.032 (0.003)	2.1 (0.1)	1.8 (0.1)	2.1	
10	G1C	1579.87	1588.22 (0.16)	12%	3.60 (0.37)	0.309 (0.020)	9.2 (0.5)	1.3 (0.4)	0.5	11
	WT		1588.00 (0.09)		8.10 (1.57)	0.096 (0.015)	6.1 (0.4)	4.2 (0.3)	0.7	
11	G1C	1719.01	1725.15 (0.13)	13%	6.15 (1.04)	0.038 (0.006)	4.1 (0.4)	3.7 (0.2)	5.2	13
	WT		1724.20 (0.16)		1.70 (0.38)	0.031 (0.010)	4.2 (0.4)	2.5 (0.3)	6.3	
13	G1C	769.77	772.83 (0.07)	16%	6.77 (1.47)	0.050 (0.010)	2.0 (0.2)	2.0 (0.1)	2.0	6
	WT		772.74 (0.11)		8.46 (2.54)	0.031 (0.012)	2.2 (0.3)	1.7 (0.2)	2.1	
13/14	G1C	986.08	989.67 (0.10)	21%	7.41 (2.28)	0.034 (0.006)	2.0 (0.3)	3.0 (0.2)	3.0	8
	WT		988.82 (0.16)		8.54 (3.80)	0.034 (0.014)	2.0 (0.4)	1.8 (0.3)	4.2	
14/15	G1C	1192.40	1195.97 (0.12)	6%	4.44 (1.07)	0.036 (0.010)	2.3 (0.3)	1.9 (0.2)	5.8	10
	WT		1194.90 (0.15)		4.44 (4.40)	0.038 (0.035)	2.0 (0.7)	1.0 (0.3)	7.0	
15[j]	G1C	976.10	978.90 (0.10)	4%	3.40 (0.79)	0.041 (0.015)	2.0 (0.2)	1.2 (0.2)	4.8	8
	WT		978.77 (0.10)		3.40	0.085 (0.045)	1.7 (0.2)	1.4 (0.3)	4.9	
16	G1C	2263.72	2280.22 (0.21)	5%	13.5 (1.8)	0.143 (0.050)	14.4 (0.8)	5.1 (0.5)	0	19
	WT		2279.92 (0.27)		14.1 (4.9)	0.138 (0.058)	14.3 (1.2)	4.6 (0.9)	0.3	
17[f]	G1C	906.14	910.94 (0.30)	9%				5.9[f]	1.1	7
	WT		908.60 (0.40)					2.8[f]	4.2	
20	G1C	1241.51	1243.94 (0.53)	26%	3.06 (1.05)	0.054 (0.247)	2.9 (0.5)	0.9 (2.2)	6.2	10
	WT		1244.20 (0.48)		1.77 (1.21)	0.140 (0.012)	2.4 (0.7)	1.7 (0.7)	5.9	
21	G1C	1282.40	1288.79 (0.27)	9%	5.42 (1.15)	0.025 (0.031)	6.8 (0.7)	1.0 (0.5)	3.2	11
	WT	1240.37	1247.00 (0.05)		10.6 (1.3)	0.170 (0.061)	6.8 (0.3)	1.3 (0.2)	2.9	
22	G1C	807.32	810.18 (0.07)	14%	8.84 (2.36)	0.277 (0.302)	3.1 (0.4)	1.1 (0.3)	1.8	6
22/F	WT	884.40	888.48 (0.40)		8.76 (1.24)	0.006 (0.009)	4.8 (0.2)	1.0 (0.9)	1.2	7
23[g]	G1C	2129.4	2139.12 (0.12)	8%	5.95 (0.77)	0.245 (0.224)	10.2 (0.7)	1.5 (0.6)	3.2	15
	WT		2139.11 (0.21)		15.6 (4.9)	0.275 (0.091)	8.7 (1.0)	3.5 (0.4)	2.8	
24	G1C	1109.23	1113.97 (0.26)	16%	5.28 (1.18)	0.020 (0.013)	4.3 (0.5)	2.0 (0.4)	2.7	9
	WT		1113.53 (0.22)		8.58 (4.58)	0.028 (0.016)	3.7 (0.7)	2.0 (0.4)	3.3	
26	G1C	1869.18	1873.70 (0.096)	12%	10.2 (2.3)	0.132 (0.08)	4.1 (0.4)	1.6 (0.3)	6.3	12
	WT		1873.70[e]		14.8 (1.5)	0.172 (0.14)	3.8 (0.8)	1.9 (0.6)	6.3	
28[h]	G1C	584.72	586.75 (0.04)	23%	5.89 (0.70)		2.9 (0.2)		1.1	4
	WT		586.76 (0.02)		8.97 (0.68)		2.9 (0.2)		1.1	
29/30[e,g]	G1C	3557.04	3573.16 (0.81)	15%	13.6 (3.2)	0.116 (0.065)	17.2 (1.1)	3.9 (0.7)	3.9	21
	WT		3573.16		13.6	0.534 (0.274)	16.7 (1.2)	4.4 (1.0)	3.9	
32	G1C	1656.96	1663.75 (0.08)	12%	4.10 (0.65)	0.146 (0.038)	5.1 (0.4)	3.4 (0.3)	1.5	10
	WT		1663.63 (0.06)		2.65 (0.43)	0.084 (0.021)	5.9 (0.3)	2.6 (0.4)	1.5	
34/35	G1C	3029.59	3040.40 (0.14)	9%	4.67 (0.50)	0.066 (0.012)	7.9 (0.4)	5.1 (0.3)	11.0	24
	WT		3040.25 (0.27)		4.86 (1.40)	0.044 (0.014)	7.9 (0.9)	5.1 (0.6)	11.0	
36	G1C	1094.2	1098.53 (0.08)	14%	3.31 (0.61)	0.067 (0.020)	3.7 (0.3)	1.9 (0.3)	2.4	8
	WT		1098.29 (0.08)		2.69 (0.53)	0.022 (0.012)	4.1 (0.3)	1.5 (0.2)	2.4	
37	G1C	806.93	809.98 (0.08)	16%	3.96 (1.35)	0.081 (0.027)	2.0 (0.3)	2.0 (0.3)	2.0	6
	WT		809.98 (0.08)		3.21 (0.71)	0.042 (0.011)	2.3 (0.2)	1.7 (0.2)	2.0	
37/38	G1C	1098.25	1103.84 (0.10)	14%	3.37 (0.56)	0.047 (0.004)	4.0 (0.3)	3.3 (0.2)	1.7	9
	WT		1103.34 (0.07)		4.31 (0.73)	0.053 (0.009)	3.9 (0.3)	2.7 (0.2)	2.4	
39[i]	G1C	1463.59	1470.75 (0.24)	13%	5.25 (1.15)	0.046 (0.075)	8.3 (0.9)	1.0 (0.7)	2.7	12
	WT		1470.75		9.25 (1.57)	0.032 (0.019)	8.0 (0.4)	1.3 (0.3)	2.7	

[a] Table lists least-squares parameter values and standard errors in parentheses. Least squares for peptides 2, 4, 6′, 12, 26, 27, 30, 31, 32, and 33 did not converge. Incompletely digested peptides were of weak intensity: 7/8, 7/F, 8/9, 9/10,12,17/18/19/20. In no cases were differences in exchange observed for these peptides between MKK1-WT and MKK1-G1C. [b] Back-exchange measured as described in Methods and Materials. [c] Parameters corrected for dilution and back-exchange: parameter (corrected) = 100[parameter/(100 − BE)0.9]. [d] $C = [Y_\infty - (A + B)]$. [e] For WT data, N and k_1 were fixed and remaining parameters were fit by least-squares. [f] Insufficient data to obtain good fit. Equilibrium mass was averaged from data points taken at times between 100−250 min. There was little detectable incorporation at short times; therefore, it was assumed that all observed incorporation reflects the intermediate rate class. [g] Weak ion, high intrinsic error. [h] Data best fit to single exponential. [i] For WT data, N was fixed and remaining parameters were fit by least-squares. [j] Peptide mass not at equilibrium after 4 h (contains His); therefore, B parameter is poorly fit. To obtain a good fit for WT, k_1 was fixed, and remaining parameters were fit by least-squares. [k] Peptide was lower in yield when derived from G1C than WT; therefore, error for G1C is greater than WT data.

peptide 13/14 is converted to an intermediate exchanging amide.

Homology Model for MKK1. A crystallographic structure for MKK1 has not been reported; therefore, a backbone conformation was approximated by sequence alignment of MKK1 against cAMP-dependent kinase (cAPK), for which several three-dimensional structures are known (Figure 4A). On the basis of comparisons between several protein kinase

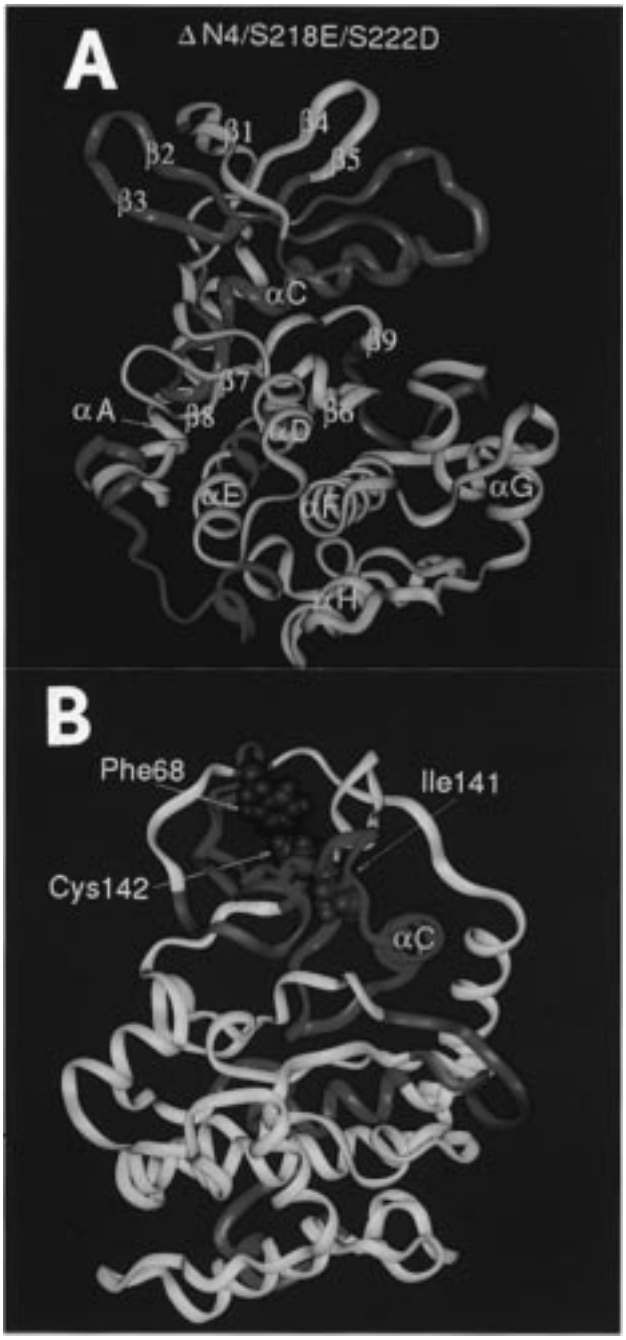

FIGURE 4: Approximation of peptide backbone structure for MKK1 based on homology mapping against cAPK. Peptides that show increased exchange upon enzyme activation by G1C mutations are colored red and those with decreased exchange are green. (A) The model shows expected structural features of the conserved kinase domain, including the N-proximal lobe composed of a five-stranded antiparallel β sheet (β1−β5) with underlying α helix C, and the C-proximal lobe with five α helices (D−H), containing the substrate binding site. An active site cleft formed between the lobes presents conserved aspartate residues within four short β strands (β6−β9) for metal coordination and base-assisted catalysis and provides contacts from the N-proximal lobe for ATP binding. (B) Alternative view, illustrating predicted contacts between Phe68 and Cys142 and Ile141 and α helix C.

structures (*3*, *4*), this homology model should provide a reasonable approximation of MKK1 in conserved helices C-F and β strands 1−9, with higher uncertainty within loops between helices or β strands and in N- and C- terminal regions outside the conserved kinase core. Minor additions or deletions were made as described in Materials and Methods, in order to optimize the alignment, and a 42 amino acid insert, which is unique to MKK, was removed between subdomains 9 and 10. MKK1 residues 42−58, which includes the ΔN4 deletion (residues 44−51), were aligned with the A helix of cAPK (*23*, *24*). The conserved secondary structural features characteristic of kinases as observed in MKK1 are indicated in Figures 1 and 4A. The energy minimized model showed few changes from cAPK, except for helix B of cAPK, which was converted to a random coil in the MKK1 model. In particular, the model retained A helix and the cAPK tertiary conformation within the activation lip between subdomains 7 and 8 (residues 216−225).

Overall, comparison of in-exchange with the predicted secondary structure did not show any clear correlation of α helices or β sheets with the overall exchange rates. Peptides predicted to be completely buried in MKK1 showed low levels of in-exchange; for example, peptides 17 and 20 exchanged only 30−40% after 4 h (Table 1). Peptide 17 includes the C-terminal region of helix E and is buried at the interface between the N- and C-proximal lobes (Figure 4A). No significant exchange was observed at short times (<15 s), indicating that this peptide has no fast exchanging amides; therefore, the exchanging amides are in the intermediate class, consistent with models that suggest that intermediate amides do not have ready access to solvent. This peptide was low in intensity and frequently was not seen. Nevertheless, comparison of the masses at long incubation times showed a large (2 Da) increased deuterium exchange into peptide 17 in G1C compared to WT (Table 1), indicating conversion of two slow to two intermediate exchanging amides. Peptide 17 is part of a hydrophobic core resistant to digestion; the incompletely proteolyzed peptide 17/18/19/20 that also showed low in-exchange was recovered. The large size of this core peptide made detailed analysis problematic.

Other peptides in MKK1 that underwent changes in deuterium in-exchange between WT and G1C are shown in Figure 4. The peptides that showed decreases in exchange rate upon activation are located within the glycine-rich ATP binding loop, the Asp_{208} Mg^{2+} coordination site, and the activation lip (colored green in Figure 4). Peptides showing increases in exchange rate (colored red in Figure 4) were found in the N-proximal lobe including the five-stranded β sheet and helix C, peptide 17, and two peptides in the C-proximal lobe. The separate contributions of each mutation were examined by additional experiments analyzing MKK1 mutants containing the N-terminal deletion (ΔN4) or the phosphorylation site substitutions at the activation lip (S218E/S222D) (results summarized in Figure 5 and Table 2).

ATP Binding Region. Peptides 6/F, 8, 9, 10, 11, 13/14, and 14/15, derived from the β sheet in the N-proximal lobe (β1−β5), all show increased in-exchange in comparing WT to G1C (Figures 3, 6, and 7). As described below, most of these increases fit simple models where 1−2 amides in each peptide underwent alterations in exchange rate. This interpretation was supported by three examples of peptides where alternative proteolytic cleavages resulted in products differing by 1−2 residues (6 vs 6/F; 13 vs 13/14; 14/15 vs 15), pinpointing specific amide residues that were altered in their exchange rate.

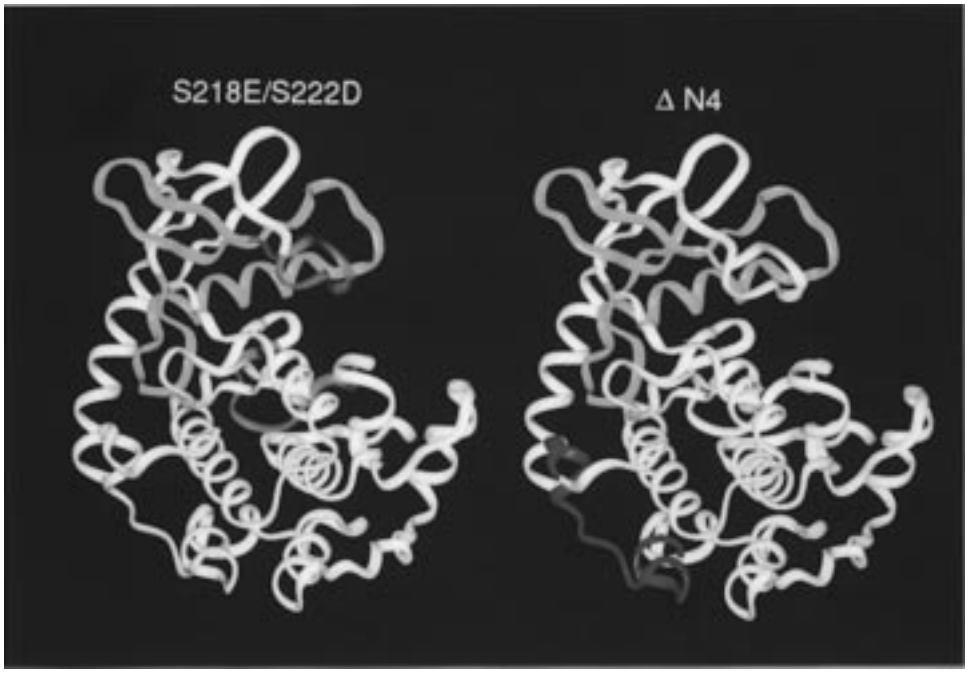

FIGURE 5: Changes in exchange rate into constitutively active MKK1 containing individual mutations. Colors show peptides that undergo altered exchange rates upon enzyme activation by S218E/S222D or ΔN4 mutations. Peptides with increased exchange are red and decreased exchange are green. Peptides with increased exchange that are intermediate to the levels achieved in G1C are pink.

Table 2: Exchange Behavior of Peptides from MKK1 Mutants Compared to MKK1-WT

peptide	conserved subdomain/sequence	MKK1-G1C	MKK1-S218E/S222D	MKK1-ΔN4
6	β1	++++	no change	++
7b	GxGxxG ATP binding loop	-	-	no change
8	β2-loop-β3	++	+	+
9	β3/ Lys_{97} ion pair with ATP	++++	++	++
10	αC/Glu_{114} ion pair with Lys_{97}	++	+	+
11	αC-loop-β4	++++	++	++
14	β5	++++	no change	++
17	helix E	++++	not determined	not determined
21	β9/Mg^{2+} coordination	---	---	no change
22	Activation lip/Ser_{218}, Ser_{222}	----	----	no change
38	C-terminus (not conserved)	+	no change	+

Peptides 13/14 and 14/15 showed increased exchange in G1C (Figure 3, panels A and C), whereas peptides 13 and 15 remained unchanged (Figure 3, panels B and D), thus the altered amide must be located within the sequence Ser_{140}-Ile-Cys-Met in the β5 strand. Whereas peptide 13/14 fits to two fast, two intermediate, and four slow amides (2F/2I/4S) in WT and 2F/3I/3S in G1C (Table 1), peptide 13 fits to 2F/2I/2S for both WT and G1C, implying that Ser_{140}-Ile and Ile_{141}-Cys amides are slow exchanging in WT and that one becomes intermediate exchanging in G1C. This rate enhancement is greater than 35-fold, assuming that the slow amides have rates less than 0.001 min^{-1}. Similarily, peptide 14/15 fits to 2F/1I/7S vs 2F/2I/6S for WT vs G1C whereas peptide 15 fits to 2F/1I/5S for both proteins (Table 1), indicating that Ile_{141}-Cys and Cys_{142}-Met amides are both slow exchanging in WT and that one becomes intermediate exchanging in G1C. Together, these data indicate that the Ile_{141}-Cys amide accounts for the major part of the change. However, the normalized difference between WT and G1C in equilibrium mass (*N*) for peptide 14/15 is approximately 1.3−1.4 Da, suggesting that the Cys_{142}-Met amide also undergoes a small rate increase. A major change at this site is also indicated by differential recovery of these peptides from each protein (data not shown), consistent with a slight preference for proteolysis of the Cys-Met bond in G1C.

In a second example, peptide 6/F showed enhanced in-exchange between WT and G1C, whereas peptide 6 showed no obvious differences (Figure 6). This suggests that the enhancement occurs specifically at the Asp_{67}-Phe amide (in the β1 strand). Although Table 1 suggests a change in two amides, the large peptide size introduces higher parameter errors; visual inspection of Figure 6A suggests that the data most likely signifies a single intermediate exchanger in WT that becomes a fast exchanger in G1C. Interestingly, Cys_{142} in β5 forms contacts with Phe_{68} in β1 in the homology model, suggesting that the altered exchange rates in peptide 6 and 14/15 may be coupled (Figure 4B).

Possible coupling of peptide 14/15 to helix C is suggested by the increases in peptide 10 and 11 (Figure 7, panels C and D). Peptide 11 contains the C-terminal portion of helix C, the N-terminal portion of the β4 strand, and the intervening loop between these sequences. In the homology model, it forms hydrophobic contacts (Leu_{115} and Leu_{118} of helix C and Val_{127}, Gly_{128}, and Phe_{129} of β4) with Ile_{141} and Met_{143} in the β5 strand. The normalized *B* parameter for peptide 11 was greater in G1C by 1.3 Da, and the *C* parameter was

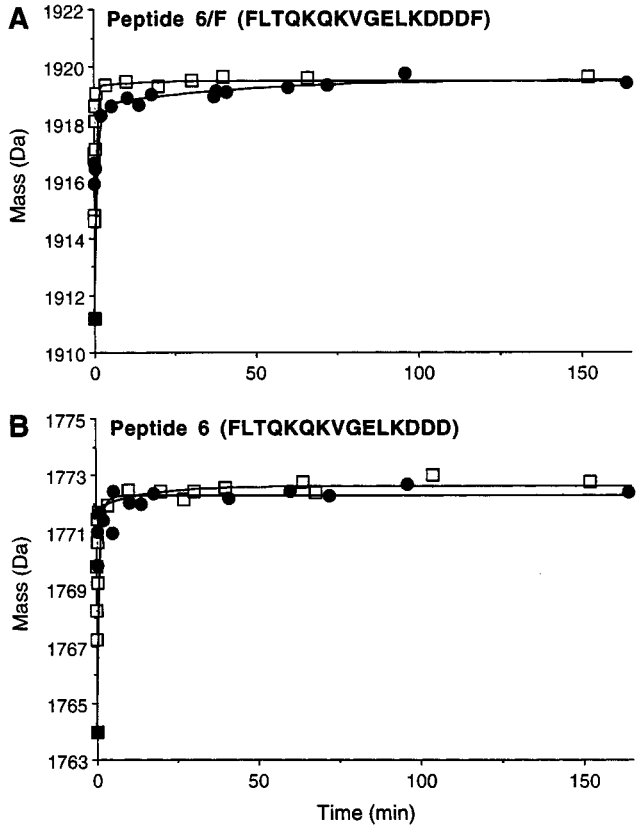

FIGURE 6: Deuterium incorporation into alternatively proteolyzed forms demonstrate that enhanced deuteration in G1C can be localized to Asp_{67}-Phe. Time courses are shown for alternatively proteolyzed forms of (A) peptide 6/F or (B) peptide 6 derived from WT (●) or G1C (□). Masses were averaged from MH_2^{2+} and MH_3^{3+} ions for peptide 6/F and the MH_2^{2+} ion for peptide 6. Data are presented as in Figure 3. The error in mass for peptide 6 is larger because the ion intensity is weaker than peptide 6/F. Note that the scale on the *y*-axis is approximately half that in Figure 3, so that the maximal difference between WT and G1C is 1 Da in panel A.

smaller by 1.2 Da, so that the simplest model is a conversion of a slow exchanging amide to an intermediate exchanging amide upon activation. Peptide 10 contains the remainder of helix C, including a conserved Glu_{114} residue found in all protein kinases, which forms a salt bridge with a conserved Lys97 in β3 (*3*). In the homology model, this peptide forms contacts between helix C and β5. The mass increase after 4 h was 10.4 Da, thus the exchange among 11 available amides was nearly complete, indicating that solvent access to this peptide is high. Changes in fitted parameters were complex and are not interpretable as simple effects on single amides.

The last two peptides that show increases are peptides 8 and 9, which contain residues in β2 and β3 and the loop between them (Figure 7, panels A and B). The fitted data for peptide 8 (containing residues in β2 and β3 and the loop between them) indicates that one or two amides shift from the intermediate class in WT to the fast class in G1C. In contrast, the fitted data for peptide 9 (containing part of β3 and Lys_{97}, the predicted salt bridge pair to Glu_{114}) indicated no difference in the number of amides in each class. However, k_2 in G1C was 5-fold greater than in WT (Table 1); because the *B* parameter was approximately equal to 2, the simplest model would have one or both of the intermediate exchanging amides undergoing increased exchange rates.

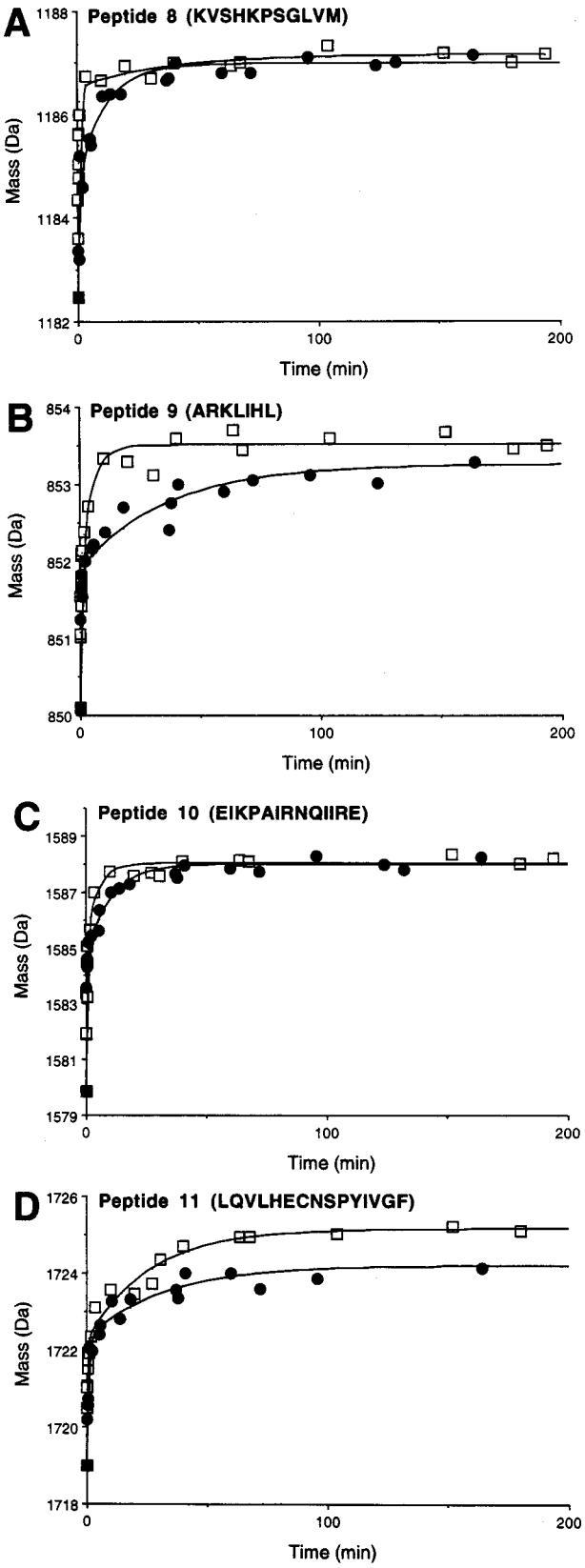

FIGURE 7: Deuterium incorporation demonstrating enhanced exchange into G1C. Time courses are shown for (A) peptide 8, (B) peptide 9, (C) peptide 10, or (D) peptide 11 derived from WT (●) or G1C (□). Peptide 11 did not reach equilibrium in 4 h. Data are presented as in Figure 3.

Examination of the S218E/S222D and ΔN4 constitutively active mutants showed enhanced deuterium exchange rates in the same peptides within the N-proximal lobe (Figure 5,

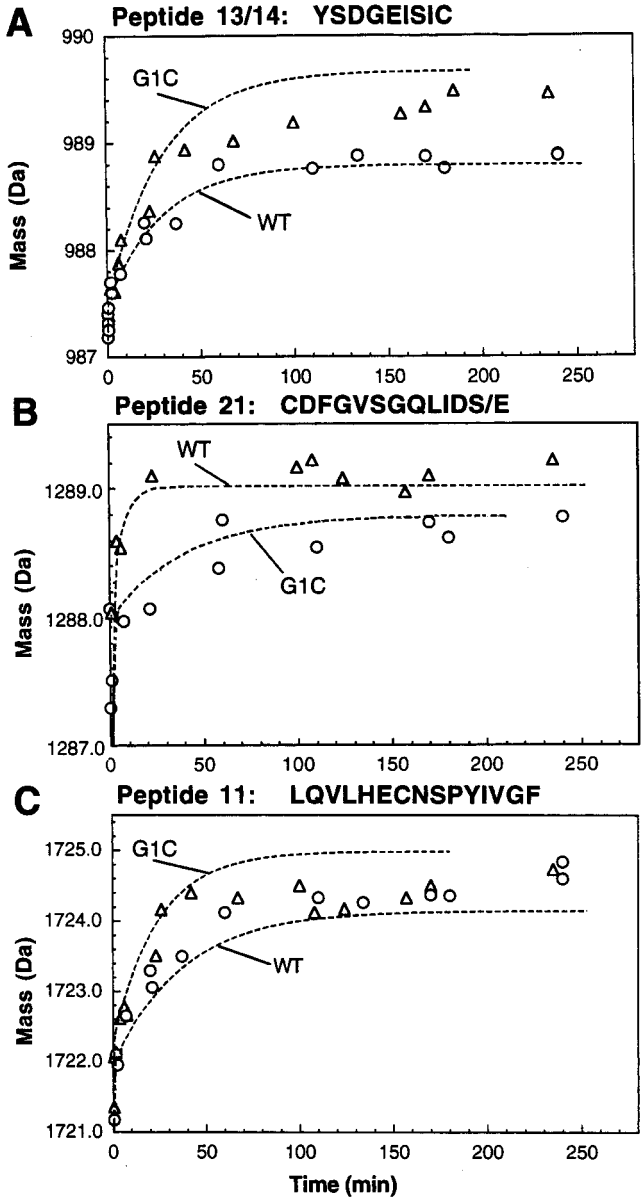

FIGURE 8: Variable changes in exchange rates observed in constitutively active MKK1 containing individual mutations. Time courses of deuterium exchange into (A) peptide 13/14, (B) peptide 21, or (C) peptide 11, derived from ΔN4 (△) or S218E/S222D (○). Dotted lines indicate the time courses for the corresponding peptides derived from WT or G1C (taken from Figures 3A, 9B, and 7D). (A) The data for S218E/S222D (○) resemble the WT time course, while the ΔN4 data (△) were intermediate between the G1C and WT time courses. (B) The data for S218E/S222D (○) resemble the G1C time course, while the ΔN4 data (△) resesmble the WT. (C) The data for S218E/S222D (○) and ΔN4 data (△) were intermediate between the G1C and WT time courses.

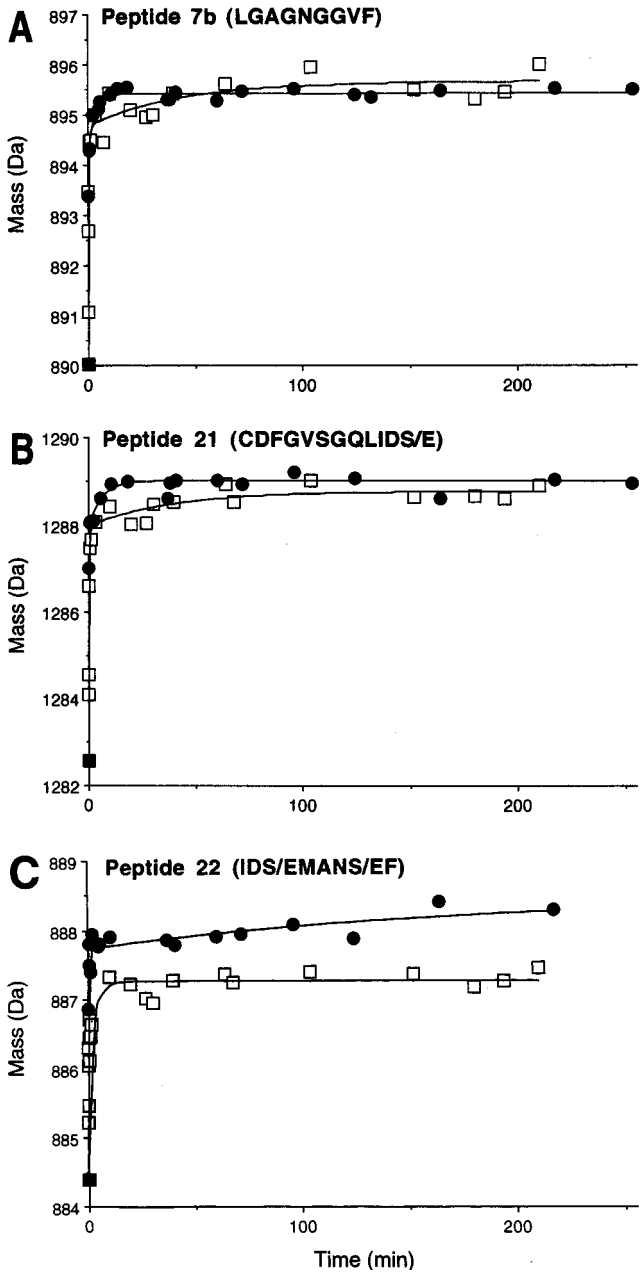

FIGURE 9: Deuterium incorporation demonstrating decreased exchange into G1C. Time courses are shown for (A) peptide 7b and (B) peptide 21, derived from WT (●) or G1C (□). Peptides 21 and 22 differed in mass between WT and G1C due to mutations at Ser_{218} and Ser_{222}. Peptide 22 also showed alternative cleavages at Phe_{223} in WT vs Asp_{222} in G1C, so that peptide 22 derived from G1C does not have the C-terminal Phe. Therefore data sets from WT and G1C were adjusted to the same scale by adding constant masses calculated from the differences between average masses in water. Peptide 21 is shown with constant mass of 42.03 Da added to WT values (panel B), and peptide 22 is shown with constant mass of 77.08 Da added to G1C values (panel C). Mutated residues are indicated as S/E or S/D.

Table 2). When comparing peptides 13/14, 14/15, and 6/F derived from WT and ΔN4, enhanced in-exchange was observed for the active mutant, but the magnitude was intermediate to that seen with G1C. In contrast, the behavior of these three peptides when derived from S218E/S222D was identical to that seen in WT (shown for peptide 13/14, Figure 8A). These may constitute functionally coupled contacts, given that the acidic replacements do not affect them, while the ΔN4 deletion does. Peptides 8, 9, and 11 all showed enhanced exchange with either mutant, with magnitude intermediate to that observed with G1C (Figure 5; data shown for peptide 11, Figure 8C). Data from ΔN4 and S218E/S222D mutants were difficult to analyze because the mass differences between peptide 10 from G1C vs WT were relatively small; however, they suggested deviations from WT that were intermediate to that observed with G1C (Figure 5).

Only one peptide within the N-proximal lobe showed an overall decrease in exchange between inactive and active MKK1 (Figure 9A). Peptide 7b contains the sequence motif,

GXGXXG, conserved in nearly all protein kinases, which forms a loop contacting the β and γ phosphates of ATP and covering the nucleotide (*3*, *25*). As expected, solvent access to this region was high, with an estimated seven out of eight available amides exchanging within 4 h. Fitted values revealed a complex behavior of this peptide, but modeling indicates that most of the decreased exchange can be attributed to a 20-fold decreased k_2. Fitted parameters for peptide 7b derived from S218E/S222D resembled those derived from G1C. In contrast, parameters for ΔN4 resembled those from WT, suggesting that the changes observed in G1C were mostly due to acidic residue substitutions at the phosphorylatable Ser residues (Figure 5, in green).

Activation Lip Region. Peptides 21 and 22 both showed decreased exchange in G1C relative to WT (Figure 9B). Peptide 21 partially overlaps peptide 22 in the activation lip at Ser_{218} and also contains sequences within the catalytic cleft, including the β9 strand and residue Asp_{208} which functions as a Mg^{2+} coordination site. For peptide 21, the main difference between the two proteins was in the magnitude of k_2, which decreased by 7-fold from WT to G1C. The best fit showed a single intermediate exchanging amide; therefore, the primary rate change most likely occurred at this intermediate amide. Peptide 22 contains both Ser_{218} and Ser_{222}, and thus spans a critical portion of the activation lip. The S218E/S222D mutation in G1C altered the site of pepsin cleavage in the activation lip (Figure 1). Thus, peptides with sequence $IDE_{218}MAND_{222}$ (peptide 22) and $IDS_{218}MANS_{222}F$ (peptide 22/F) were recovered from G1C and WT, respectively (Figure 9, panels B and C). Fitted parameters for IDSMANSF indicated 5F/1I/1S out of seven exchangeable amides (Table 1). In contrast, fitted parameters for IDEMAND indicated 3F/1I/2S out of six exchangeable amides. It is not possible to account for this magnitude of change by the addition of one amide; therefore, the region encompassing IDEMAND must include at least one amide with a decreased rate.

Taken together, these data suggest large decreases in exchange rates for at least 2 amides within the activation lip region. The expected change in intrinsic exchange rate upon replacement of Ser with Glu or Asp are not sufficient to account for these decreases. Similar reductions in exchange rates for both peptides 21 and 22 were observed in S218E/S222D; however, exchange rates in this region were unaffected by ΔN4 (shown for peptide 21, Figure 8B). Thus, the decreased exchange in the activation lip could be attributed entirely to the acidic amino acid substitutions.

C-Terminal Sequences outside the Kinase Core. Minor increases in deuterium incorporation were observed in C-terminal peptides 36 and 37/38, comparing G1C to WT. In contrast to the small increase in 37/38 (0.5 Da at 4 h), peptide 37 showed little difference between WT and G1C, indicating that the change in exchange in peptide 37/38 occurs within the sequence Leu_{375}-Cys-Ser-Thr. The small change in peptide 36 appeared as a barely significant increased value of k_2 (Table 1). Originally it was discounted; however, a similar small increase was observed in peptide 36 derived from ΔN4, but not S218E/S222D. In the homology model, peptide 36 spans helix I, which is found in most protein kinase structures at the base of the C-proximal lobe on the side opposite to the catalytic cleft (*3*). This peptide is in contact with helix A, suggesting that the changes might be due to a disruption of contacts due to shortening of helix A. This is further supported by the fact that the changes in peptide 37/38 also occurred only in the ΔN4 mutant.

DISCUSSION

Using an improved protocol for deuterium exchange mass spectrometry, which enhances resolution by reducing the back exchange of deuterium for hydrogen, significant differences were revealed between wild-type MKK1 and two distinct, but synergistic, activating mutations. Decreased exchange rates were detected near the activation lip in mutants where the phosphorylation sites were replaced by acidic residues. Because previous results show that introduction of negative charge at the activation lip is a key component of the activation mechanism (*7*), the decreased exchange may involve new electrostatic interactions introduced by mutagenesis. Conformational rearrangement of the lip by formation of new salt and hydrogen bonds is observed in X-ray structures of protein kinases that are activated by protein phosphorylation (*5*, *26*), although effects due to electrostriction cannot be ruled out. In addition, a small decrease in exchange rate was observed in the glycine-rich ATP binding loop, and the activated enzyme showed increased stability to shear denaturation. These results are consistent with the prevailing model for protein kinase activation, which postulates a domain closure through rotation of the N-proximal lobe with respect to the C-proximal lobe (*5*, *8*). However, increased hydrogen exchange was also detected within the interface between the two lobes, indicating that a more complex model for activation is required.

Unexpectedly, a wide-spread increase in exchange was observed in the five-stranded β sheet of the N-proximal lobe and in helix C that buttresses it (peptides 6, 8, 9, 10, 11, and 14/15). For most of these peptides, curve fitting and modeling indicated that the increases in rate could be attributed to one or two amides in each peptide. This was most clearly shown in two peptides with alternative cleavage sites, where the enhanced exchange was localized to specific amides between Asp_{67}-Phe on β1 and Ile_{141}-Cys on β5. Because these changes apparently occur at specific amides, the results are most compatible with enhanced formation of mobile defects that are large enough to allow diffusion of water molecules into the N-proximal lobe (*27*, *28*), rather than large unfolding events or rigid body movements.

These effects may be due to enhanced dynamic motion and flexibility within the N-proximal lobe. Because the N-proximal lobe provides extensive contacts with ATP (*3*, *25*), enhanced flexibility in the activated mutants could facilitate the conformational changes involving ATP binding, phosphoryl transfer, and ADP release. This hypothesis is consistent with kinetic studies on cAPK showing that ADP release is rate limiting during catalysis (*29*). In addition, the ΔN4 deletion and the acidic amino acid substitutions in the activation lip both led to increased exchange in this region that was intermediate to that seen with G1C. Thus, combining these mutations enhances both deuterium exchange and enzymatic activity (*7*), suggesting that synergy in flexibility within the β sheet/helix C domain may account for the corresponding synergistic effects on activation.

A reasonable model to explain the activation of MKK1 by mutagenesis invokes a network of residue interactions that allows communication between mutated residues and helix C. X-ray structures of protein kinases show ionic interactions between phosphorylated amino acids within the activation lip and basic residues in helix C (*5*, *26*, *30*, *31*). Substitution of phosphorylated residues with acidic amino acids may elevate activity by mimicking such interactions (*7*). In a similar manner, activation of MKK1 by the ΔN4 mutation may involve interactions between the N-proximal lobe and helix C. This is based on the alignment between the N-terminal helix A of cAPK and a predicted helical domain within residues 44−51 of MKK1 (*6*), where Trp_{30} in helix A of cAPK forms cation−π interactions with Arg_{93} in helix C and Arg_{190} in β9 of the catalytic domain (*32*). Our previous studies indicate that the ΔN4 deletion elevates kinase activity by disrupting constraints in secondary structure (*7*).

The increased flexibility observed in the N-proximal lobe could be coupled by a network of interactions between the N-terminal β sheet and helix C, which are predicted from the homology model of MKK1. Thus, helix C may be a key transducing element, enabling conformational changes at the activation lip and N-terminus of MKK1 to enhance the dynamic motions within the N-proximal lobe and thus increase activity. Synergistic activation by the two types of mutations might occur as a result of electrostatic interactions between the activation lip and helix C, along with perturbations of helix C and helix A interactions introduced by the ΔN4 deletion. Deuterium exchange work is under way to determine whether mechanisms of activation by mutagenesis are comparable to physiological activation by phosphorylation and to compare these effects with other regulatable kinases.

The importance of local changes in protein flexibility in enzyme catalysis are assumed in classic models for induced fit or allosteric enzyme regulation (*33*). However, few examples exist, verifying the influence of dynamic motion on catalysis by direct experimentation. Current ideas about enzymatic reactions postulate fluctuational movements in enzymes that enable crossing of energy barriers along reaction coordinates. This study implicates enhanced flexibility within a localized subdomain in enzymatic catalysis, but points to enhanced formation of mobile defects, rather than large body movements. An increase in mobile defects in MKK1 upon activation suggests an increase in molecular volume of the kinase. These effects are consistent with studies on enzyme compressibility showing that increased compressibility (i.e., increased molecular volume) can be correlated with activity of various enzyme mutants, even in cases where differences are not apparent by X-ray crystallography (*34*). Thus, deuterium exchange studies of regulatable protein kinases may provide unique experimental insight into the dynamic motions required for enzyme catalysis.

ACKNOWLEDGMENT

We are grateful to Richard Johnson and Arthur Pardi for innumerable conversations about deuterium exchange and mass spectrometry and to Susan Taylor for X-ray coordinates of cAMP-dependent protein kinase and valuable insights into protein kinase structure. We also thank Deborah Wuttke and Arthur Pardi for their generous help with InsightII and Greg Aiollo of PE Sciex for outstanding maintenance of our mass spectrometer.

REFERENCES

1. Seger, R., and Krebs, E. G. (1995) *FASEB J. 9*, 726−735.
2. Lewis, T. S., Shapiro, P. S., and Ahn, N. G. (1997) *Adv. Cancer Res.* (in press).
3. Taylor, S. S., and Radzio-Andzelm, E. (1994) *Curr. Biol. 2*, 345−355.
4. Goldsmith, E. J., and Cobb, M. H. (1994) *Curr. Opin. Struct. Biol. 4*, 833−840.
5. Johnson, L. N., Noble, M. E. M., and Owen, D. J. (1996) *Cell 85*, 149−158.
6. Mansour, S. J., Matten, W. T., Hermann, A. S., Candia, J. M., Rong, S., Fukasawa, K., Vande Woude, G. F., and Ahn, N. G. (1994) *Science 265*, 966−970.
7. Mansour, S. J., Candia, J. M., Matsuuda, J., Manning, M., and Ahn, N. G. (1996) *Biochemistry 35*, 15529−15536.
8. Cox, S., Radzio-Andzelm, E., and Taylor, S. S. (1994) *Curr. Opin. Struct. Biol. 4*, 893−901.
9. Frauenfelder, H., Sligar, S. G., and Wolynes, P. G. (1991) *Science 254*, 1598−1603.
10. Cannon, W. R., Singleton, S. F., and Benkovic, S. J. (1996) *Nat. Struct. Biol. 3*, 821−833.
11. Englander, S. W., and Kallenbach, N. R. (1984) *Q. Rev. Biophys. 16*, 521−655.
12. Gregory, R. B., and Rosenberg, A. (1986) *Methods Enzymol. 131*, 448−517.
13. Englander, S. W., and Mayne, L. (1992) *Annu. Rev. Biophys. Biomol. Struct. 21*, 243−65.
14. Zhang, Z., and Smith, D. L. (1993) *Protein Sci. 2*, 522−531.
15. Johnson, R. S., and Walsh, K. A. (1994) *Protein Sci. 3*, 2411−2418.
16. Smith, D. L., and Zhang, Z. (1994) *Mass Spectrom. Rev. 13*, 411−429.
17. Mansour, S. J., Resing, K. A., Candia, J. M., Hermann, A. S., Gloor, J. W., Herskind, K. R., Wartmann, M., Davis, R. J., and Ahn, N. G. (1994) *J. Biochem. 116*, 304−314.
18. Resing, K. A., Mansour, S. J., Hermann, A. S., Johnson, R. S., Candia, J. M., Fukasawa, K., Vande Woude, G. F., and Ahn, N. G. (1995) *Biochemistry 34*, 2610−2620.
19. Knighton, D. R., Zheng, J., Ten Eyck, L. F., Xuong, N.-H., Taylor, S. S., and Sowadski, J. M. (1991) *Science 253*, 414−420.
20. Zhang, Z., Post, C. B., and Smith, D. L. (1996) *Biochemistry 35*, 779−791.
21. Bai, Y., Milne, J. S., Mayne, L., and Englander, S. W. (1993) *Proteins* 17, 75−86.
22. Raussens, V., Narayanaswami, V., Goormaghtigh, E., Ryan, R. O., and Ruysschaert, J.-M. (1996) *J. Biol. Chem. 271*, 23089−23095.
23. Veron, M., Radzio-Andzelm, E., Tsigelny, I., Ten Eyck, L. F., and Taylor, S. S. (1993) *Proc. Natl. Acad. Sci. U.S.A. 90*, 10618−10622.
24. Zheng, J, Knighton, D. R., Zuong, N.-H., Taylor, S. S., Sowadski, J. M., and Ten Eyck, L. F. (1993) *Protein Sci. 2*, 1559−1573.
25. Bossemeyer, D. (1994) *Trends Biochem. Sci. 19*, 201−205.
26. Jeffrey, P. D., Russo, A. A., Polyak, K., Gibbs, E., Hurwitz, J., Massagué, J., and Pavletich, N. P. (1995) *Nature 376*, 313−320.
27. Richards, F. M. (1979) *Carlsberg Res. Commun. 44*, 47−63.
28. Miller, D. W., and Dill, K. A. (1995) *Protein Sci. 4*, 1860−1873.
29. Adams, J. A., and Taylor, S. S. (1992) *Biochemistry 31*, 8516−8522.
30. Owen, D. J., Noble, M. E., Garman, E. F., Papageorgiou, A. C., and Johnson, L. N. (1995) *Structure 3*, 467−482.
31. Knighton, D. R., Zheng, J., Ten Eyck, L. F., Ashford, V. A., Xuong, N.-H., Taylor, S. S., and Sowadski, J. M. (1991) *Science 253*, 407−414.

32. Herberg, F. W., Zimmermann, B., McGlone, M., and Taylor, S. S. (1997) *Protein Sci. 6*, 569−579.
33. Koshland, D. E. (1987) *Cold Spring Harbor Symp. Quant. Biol. 52*, 1−7.
34. Gekko, K., Tamura, Y., Ohmae, E., Hayashi, H., Kagamiyama, H., and Ueno, H. (1996) *Protein Sci. 5*, 542−545.

BI971750X